

FOURIER DOMAIN BEAMFORMING FOR COHERENT PLANE-WAVE COMPOUNDING

Regev Cohen, Yael Sde-Chen*, Tanya Chernyakova**
*Christophe Fraschini**, Jeremy Bercoff**, Yonina C. Eldar**

* Technion - Israel Institute of Technology, Dept. of Electrical Engineering, Haifa 32000, Israel

** Supersonic Imagine, Aix-en-Provence, France

ABSTRACT

Ultrafast imaging based on coherent plane-wave compounding is one of the most important recent developments in medical ultrasound. It significantly improves image quality and allows for much faster image acquisition. This method, however, incurs severe computational loads that create a major bottleneck in its implementation using existing commercial systems. To overcome this limitation we translate the beamforming, which is the basic processing step, to the frequency domain. As a result the computations can be carried out much more efficiently and using less data samples. To this end, we extend the frequency domain beamforming (FDBF) framework developed recently for the focused imaging mode to plane-wave imaging. We show that the core of FDBF, the relationship between the beam and the detected signals in the frequency domain, holds and can be implemented efficiently by introducing an appropriate approximation. We also show that dynamic aperture and apodization, crucial for image quality improvement, can be applied directly in frequency as a part of FDBF. The translation of beamforming into the frequency domain allows for data rate reduction by eliminating oversampling, required by digital implementation of beamforming in time. As a result the signals are sampled and processed at their effective Nyquist rate, leading to a 4-fold reduction in the number of samples.

Index Terms— Array processing, ultrafast imaging, plane-wave, beamforming, ultrasound.

1. INTRODUCTION

Ultrasound is a radiation free imaging modality with numerous applications. In a standard imaging cycle a pulse of acoustic energy is transmitted along a narrow beam from an array of transducer elements. During the pulse's propagation echoes are scattered by acoustic impedance perturbations in the tissue, and detected by the elements of the transducer. Collected data is processed in a way referred to as beamforming [1], which results in signal-to-noise ratio (SNR) enhancement and improvement of angular localization. Such a beamformed signal forms a line in the image.

The number of transmissions is proportional to the number of lines since the entire image is built by repeating the above process for scanlines in all desired directions. As a result, in this approach the frame rate is defined by the time required to transmit a beam, receive and process the resulting echoes and repeat this process for all scanlines of the image. Regardless of the computational power, physical constraints imply that the time required to obtain an image is $T_{image} = \frac{N_{lines} \cdot 2 \cdot r}{c}$, where r is the penetration depth, c is the

speed of sound in the tissue and N_{lines} is the number of scanlines in the image. The maximum frame rate which can be reached with this technique is $FR = \frac{1}{T_{image}}$.

Conventional frame rates are insufficient for a number of applications including echocardiography for heart motion analysis, 3D/4D imaging, elastography and more. This motivates the development of tools for frame rate improvement without compromising image quality. The key to such an improvement is to break the link between the number of transmissions and image lines.

An obvious way to reduce the number of transmissions is to insonify the entire scene with a pulsed plane-wave, while all the image lines are obtained in parallel from the acquired data by standard beamforming upon reception. This approach was successfully applied by Fink and co-authors [2], [3] for real-time imaging of the propagation of shear mechanical waves, implying ultrafast frame rates. However, due to inherent lack of the focusing step upon transmission, this method suffers from reduced contrast and resolution. This limitation can be overcome by sequential transmission of several tilted plane-waves [4]. The images obtained from each insonification are added coherently to yield a final compounded image. Such an image is characterized by significantly improved resolution and contrast since coherent compounding effectively generates a posteriori synthetic focusing in the transmission [4].

Although improving the frame-rate while retaining optimal image quality, the above method is limited by severe computational loads that create a major bottleneck for its implementation in existing commercial systems. In this work, we propose a solution for the computational complexity problem based on frequency domain beamforming (FDBF) developed recently for the focused imaging mode. As shown in [5], in this domain the computations can be carried out much more efficiently and from less data samples. We therefore extend FDBF to plane-wave imaging and show that it can be implemented efficiently by introducing an appropriate approximation. We also show that dynamic aperture and apodization, crucial for image quality improvement, can be applied directly as part of FDBF. Translation of beamforming into the frequency domain allows for data rate reduction by eliminating oversampling, required by digital implementation of beamforming in time. As a result the signals are sampled and processed at their effective Nyquist rate, leading to a 4-fold reduction in the number of samples.

The rest of the paper is organized as follows: in Section 2 we review the processing performed in plane-wave imaging. Next, in Section 3 we derive the proposed frequency domain formulation. The results obtained by applying the proposed method to data acquired by an Aixplorer scanner are presented in Section 4.

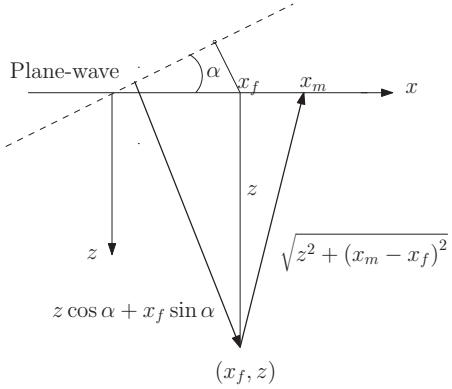


Fig. 1. Plane-wave imaging setup: a transducer is aligned along the x axis transmitting a propagating plane-wave with inclination α .

2. COHERENT PLANE-WAVE COMPOUNDING

In coherent plane-wave compounding, the final image is a result of coherently adding several images obtained by transmitting tilted plane-waves with different angles [4]. We begin with a description of the beamforming process required to obtain each one of the images being compounded.

Assume we transmit a plane-wave with inclination α as shown in Fig. 1. An echo reflected by a scatterer positioned at (x_f, z) arrives to a transducer element placed at x_m at time

$$\tau_m(z; x_f, \alpha) = \frac{1}{c} \left(z \cos \alpha + x_f \sin \alpha + \sqrt{z^2 + (x_m - x_f)^2} \right). \quad (1)$$

Beamforming involves averaging the signals detected by M transducer elements, $\{\varphi_m^\alpha(t)\}_{m=1}^M$, while compensating for the differences in arrival time. This results in a signal containing the energy reflected from the point (x_f, z) . Using (1) and substituting $z = \frac{ct}{2}$, the beamformed signal, corresponding to an image line x_f is

$$\begin{aligned} \Phi(t; x_f, \alpha) &= \sum_{m=1}^M w_m(t; x_f) \hat{\varphi}_m(t; x_f, \alpha), \\ \hat{\varphi}_m(t; x_f, \alpha) &= \varphi_m^\alpha(\tau_m(t; x_f, \alpha)), \\ \tau_m(t; x_f, \alpha) &= \frac{1}{2} \left(t \cos \alpha + 2 \frac{x_f}{c} \sin \alpha + \sqrt{t^2 + 4\delta_{fm}^2} \right), \end{aligned} \quad (2)$$

where $\delta_{fm} = |x_m - x_f|/c$ and $w_m(t; x_f)$ is a time-dependent weight-function multiplying each detected signal. Weight-functions are required to achieve dynamic aperture and apodization. Dynamic aperture ensures constant F-number, $f\#$, defined as the depth of focus in tissue divided by aperture width. This results in more homogeneous beampattern throughout the entire image depth. Dynamic apodization improves the contrast by reducing the side-lobes of the resulting beampattern. For Hamming apodization, the weights are given by

$$w_m(t; x_f) = \frac{1}{N(t; x_f)} A_m(t; x_f) I_{[4f\#\delta_{fm}; \infty)}(t) \quad (3)$$

$$N(t; x_f) = \left(\hat{\alpha}^2 + \frac{1}{2} \beta^2 \right) \frac{ct}{2f\#}, \quad \hat{\alpha} = 0.54, \beta = 0.46$$

$$A_m(t; x_f) = (\hat{\alpha} + \beta \cos(4\pi f\#\delta_{fm}/t)),$$

where $I_{[a,b]}$ is the indicator function equal to 1 when $a \leq t < b$ and 0 otherwise.

The beamforming process described in (2) is carried out digitally, rather than by manipulation of the analog signals. The signals detected at each element must be sampled at a sufficiently high rate to apply high-resolution time shifts. In practice, the signal is sampled at rates significantly higher than its Nyquist rate, in order to improve the system's beamforming resolution and to avoid artifacts caused by digital implementation of beamforming in time. Such a beamforming rate, f_s , usually varies from 4 to 10 times the transducer central frequency [6, 5]. Since all the image lines are obtained in parallel, the process described in (2) is performed hundreds of times per each plane-wave transmission. As a result, computational load is significantly increased compared to standard focused imaging, where each transmission usually requires a single beamforming step. This creates a major bottleneck in existing commercial ultrafast systems.

To reduce the load and promote real-time implementation of ultrafast imaging we adopt the ideas of beamforming in frequency. In this domain the computations can be carried out from less data samples.

3. FREQUENCY DOMAIN PROCESSING

To achieve sampling and processing rate reduction for standard focused imaging Chernyakova and Eldar [5] proposed performing beamforming in the frequency domain. In this approach the Fourier coefficients of the beam are computed as a linear combination of those of the individual detected signals, obtained from their low-rate samples. The low-rate data acquisition step is based on the ideas of Xampling [7, 8, 9], which obtains the Fourier coefficients of individual detected signals from their low-rate samples. More specifically, using Xampling we can obtain an arbitrary set κ , comprised of K frequency components, from K point-wise samples of the signal filtered with an analog kernel $s(t)$, designed according to κ . In ultrasound imaging with modulated Gaussian pulses the transmitted signal has one main band of energy. As a result the analog filter takes on the form of a band-pass filter, leading to a simple low-rate sampling scheme [5]. The choice of κ dictates the bandwidth of the filter and the resulting sampling rate.

When all the beam's Fourier coefficients within its bandwidth are computed, the sampling and processing rates are equal to the effective Nyquist rate. The beam in time is then obtained simply by an inverse Fourier transform.

In plane-wave mode the same low-rate sampling scheme can be applied to the individual signals detected by the transducer elements yielding their Fourier coefficients. We next show that the latter can be used to compute Fourier coefficients of the beam directly in frequency. Namely, we show that FDBF can be extended to plane-wave imaging and implemented efficiently using appropriate approximation.

Denote the Fourier series coefficients of $\Phi(t; x_f, \alpha)$ with respect to the interval $[0, T]$, where T is defined by the maximal imaged depth, by

$$c[k] = \frac{1}{T} \int_0^T \Phi(t; x_f, \alpha) \exp^{-i \frac{2\pi}{T} kt} dt = \sum_{m=1}^M \hat{c}_m[k]. \quad (4)$$

The second equation stems from substituting $\Phi(t; x_f, \alpha)$ by (2), while $\hat{c}_m[k]$ is given by

$$\hat{c}_m[k] = \frac{1}{T} \int_0^T w_m(t; x_f) \varphi_m^\alpha(\tau(t; x_f, \alpha)) \exp^{-i \frac{2\pi}{T} kt} dt. \quad (5)$$

Our goal is to derive a relationship between the Fourier coefficients of the beam and those of the detected signals. To this end, we substitute $x = \tau_m(t; x_f, \alpha)$. After some algebraic manipulation and replacing x by t we obtain

$$\hat{c}_m[k] = \frac{1}{T} \int_0^T \varphi_m^\alpha(t) q_{k,m}(t; x_f, \alpha) \exp^{-i\frac{2\pi}{T}kt} dt, \quad (6)$$

with

$$q_{k,m}(t; x_f, \alpha) = \frac{2f\#}{c(\hat{\alpha}^2 + 0.5\beta^2)} \cdot \frac{\sin^2 \alpha}{-y \cos \alpha + \sqrt{y^2 - 4\delta_{fm}^2 \sin(\alpha)^2}} \cdot \left[\hat{\alpha} + \beta \cos \left(\frac{4\pi f\# \delta_{fm} \sin^2 \alpha}{-y \cos \alpha + \sqrt{y^2 - 4\delta_{fm}^2 \sin^2 \alpha}} \right) \right] \cdot \frac{2}{\sin^2 \alpha} \left[\frac{y}{\sqrt{y^2 - 4\delta_{fm}^2 \sin^2 \alpha}} - \cos \alpha \right] \cdot \exp \left\{ -i\frac{2\pi}{T} k \frac{-y \cos \alpha + \sqrt{y^2 - 4\delta_{fm}^2 \sin^2 \alpha}}{\sin^2 \alpha} \right\} \cdot \exp \left\{ -i\frac{2\pi}{T} kt \right\}, \quad (7)$$

where $y = 2(t - x_f \sin \alpha/c)$. Note that the delays and weighting of every signal $\varphi_m^\alpha(t)$ are effectively applied through the distortion function $q_{k,m}(t; x_f, \alpha)$.

We next replace $\varphi_m^\alpha(t)$ by its Fourier coefficients. Denoting the n th Fourier coefficient by $c_m[n]$ we can rewrite (6) as

$$\begin{aligned} \hat{c}_m[k] &= \sum_n c_m[n] \frac{1}{T} \int_0^T q_{k,m}(t; x_f, \alpha) e^{-i\frac{2\pi}{T}(k-n)t} dt \\ &= \sum_n c_m[k-n] Q_{k,m;x_f,\alpha}[n], \end{aligned} \quad (8)$$

where $Q_{k,m;x_f,\alpha}[n]$ are the Fourier coefficients of the distortion function with respect to $[0, T]$. When substituted by its Fourier coefficients, the distortion function effectively transfers the beam-forming delays defined in (2) to the frequency domain. The function $q_{k,m}(t; x_f, \alpha)$ depends only on the array geometry and is independent of the received signals. Therefore, its Fourier coefficients can be computed off-line and used as a look-up-table (LUT) during the imaging cycle. In addition our numerical studies show that most of the energy of the set $\{Q_{k,m;x_f,\alpha}[n]\}$ is concentrated around the dc component. This behavior is typical to any choice of k, m, x_f or α and is illustrated in Fig. 2. We therefore rewrite (8) as

$$\hat{c}_m[k] \simeq \sum_{n=-N_1}^{N_2} c_m[k-n] Q_{k,m;x_f,\alpha}[n], \quad (9)$$

where the choice of N_1 and N_2 controls the approximation quality. The dependence of image quality on the number of weights $\{Q_{k,m;x_f,\alpha}[n]\}$ is demonstrated in Section 4.

Substitution of (9) into (4) yields the desired relationship between the Fourier coefficients of the beam and the individual signals

$$c[k] \simeq \sum_m \sum_{n=-N_1}^{N_2} c_m[k-n] Q_{k,m;x_f,\alpha}[n]. \quad (10)$$

Applying an inverse Fourier transform on $\{c[k]\}$ yields the beam-formed signal in time. The resulting signals are added coherently to yield a high-quality compounded image.

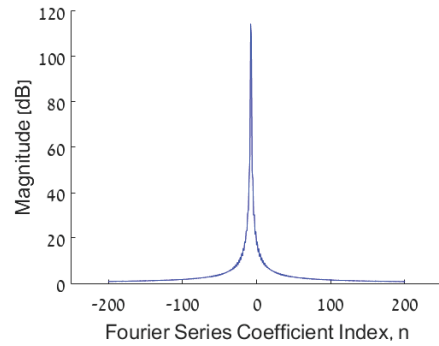


Fig. 2. Fourier coefficients $\{Q_{k,m;x_f,\alpha}[n]\}$ of $q_{k,m}(t; x_f, \alpha)$ are characterized by a rapid decay, where most of the energy is concentrated around dc component.

4. RESULTS

To verify the performance of FDBF, we simulated digitally the application of the proposed method on data obtained by an Aixplorer scanner. All the images were produced with an array of 256 elements with central frequency $f_c = 9$ MHz. Each image was obtained using 41 plane-wave transmissions with a separation of 1° . Standard time-domain processing was performed at the rate of $f_s = 36$ MHz since the rate should be 4-10 times the transducer's central frequency [6] to avoid degradation of beam quality.

For FDBF the Fourier coefficients of the beamformed signal are a combination of the Fourier coefficients of the received signals $\varphi_m^\alpha(t)$. The latter are obtained from the low-rate samples of the received signals, using the Xampling method as elaborated in Section 3. As a result FDBF is performed at the effective Nyquist rate of the signal, leading to 4-fold rate reduction.

To verify the dependence of image quality on the approximation in (9) we perform FDBF using 21, 11, 5 and 3 most significant Fourier coefficients of the distortion function $q_{k,m}(t; x_f, \alpha)$. The resulting images are shown in Fig. 3. Comparison is performed both for a single beam corresponding to an image line and for the entire image after compounding.

To compare the one-dimensional signals, we calculated the normalized root-mean-square error (NRMSE) between the signals obtained by FDBF and those obtained by standard beamforming in time. Both classes of signals were compared after envelope detection, performed by a Hilbert transform in order to remove the carrier. Denote by $\Phi[n; x_f]$ the signal obtained by standard beamforming and let $\hat{\Phi}[n; x_f]$ denote the signal obtained by beamforming in frequency. The Hilbert transform is denoted by $H(\cdot)$. For the set of J image lines, we define NRMSE as:

$$NRMSE = \frac{1}{J} \frac{\left| H(\Phi[n; x_f]) - H(\hat{\Phi}[n; x_f]) \right|_2}{H(\Phi[n; x_f])_{max} - H(\Phi[n; x_f])_{min}}, \quad (11)$$

where $H(\Phi[n; x_f])_{max}$ and $H(\Phi[n; x_f])_{min}$ denote the maximal and minimal values of the envelope of the beamformed signal in time.

Comparison of the resulting images was performed by calculating the structural similarity (SSIM) index [10], commonly used for measuring similarity between two images. Table 1 summarizes the resulting values. As can be seen, even with a very coarse approximation with only three coefficients, the images are virtually the same

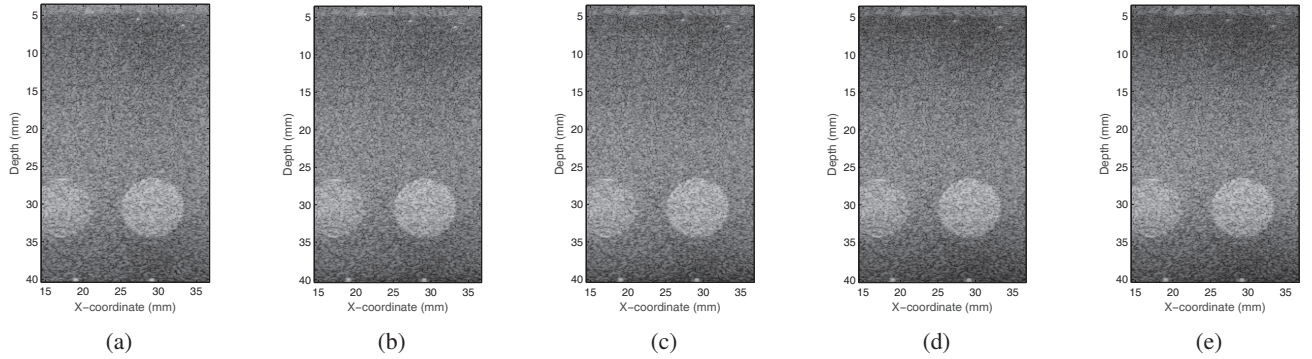


Fig. 3. Images of a calibration phantom obtained with different processing methods. (a) Time domain processing. (b)-(e) Frequency domain processing according to (10) with 21, 11, 5 and 3 coefficients $\{Q_{k,m;x_f,\alpha}[n]\}$, respectively.

Table 1. Quantitative validation of beamforming in frequency with respect to beamforming in time as a function of the number of approximation coefficients.

The number of coefficients $\{Q_{k,m;x_f,\alpha}[n]\}$	NRMSD	SSIM
21	0.072	0.95
11	0.076	0.94
5	0.0882	0.92
3	0.11	0.90

and the values of SSIM are above 0.9. Such an approximation allows for efficient implementation of low-rate FDBF, while retaining high image quality.

5. CONCLUSION

In this work we extended the frequency domain beamforming (FDBF) framework developed recently for the focused imaging mode to plane-wave imaging. We showed that the core of FDBF, the relationship between the beam and the detected signals in the frequency domain, holds and can be implemented efficiently by introducing an appropriate approximation. The dynamic aperture and apodization, crucial for image quality improvement, can be applied directly in frequency as a part of FDBF. Translation of beamforming into the frequency domain allows for data rate reduction by eliminating oversampling, required by digital implementation of beamforming in time. As a result, the signals are sampled and processed at their effective Nyquist rate, leading to 4-fold reduction in the number of samples. This approach offers a solution for the severe computational load that limits the implementation of coherent plane-wave compounding in commercial systems today.

6. REFERENCES

- [1] H. L. Van Trees, *Detection, Estimation, and Modulation Theory, Optimum Array Processing*, Wiley-Interscience, 2004.
- [2] L. Sandrin, S. Catheline, M. Tanter, X. Hennequin, and M. Fink, “Time-resolved pulsed elastography with ultrafast
- ultrasonic imaging,” *Ultrasonic imaging*, vol. 21, no. 4, pp. 259–272, 1999.
- [3] J. Bercoff, M. Tanter, and M. Fink, “Supersonic shear imaging: a new technique for soft tissue elasticity mapping,” *IEEE Transactions on Ultrasonics, Ferroelectrics and Frequency Control*, vol. 51, no. 4, pp. 396–409, 2004.
- [4] G. Montaldo, M. Tanter, J. Bercoff, N. Benech, and M. Fink, “Coherent plane-wave compounding for very high frame rate ultrasonography and transient elastography,” *Ferroelectrics and Frequency Control IEEE Transactions on Ultrasonics*, vol. 56, no. 3, pp. 489–506, 2009.
- [5] T. Chernyakova and Y. C. Eldar, “Fourier domain beamforming: The path to compressed ultrasound imaging,” *IEEE Transactions on Ultrasonics, Ferroelectrics, and Frequency Control*, vol. 61, no. 8, pp. 1252–1267, 2014.
- [6] B. D. Steinberg, “Digital beamforming in ultrasound,” *IEEE Transactions on Ultrasonics, Ferroelectrics and Frequency Control*, vol. 39, no. 6, pp. 716–721, 1992.
- [7] R. Tur, Y. C. Eldar, and Z. Friedman, “Innovation rate sampling of pulse streams with application to ultrasound imaging,” *IEEE Transactions on Signal Processing*, vol. 59, no. 4, pp. 1827–1842, 2011.
- [8] K. Gedalyahu, R. Tur, and Y. C. Eldar, “Multichannel sampling of pulse streams at the rate of innovation,” *IEEE Transactions on Signal Processing*, vol. 59, no. 4, pp. 1491–1504, 2011.
- [9] E. Baransky, G. Itzhak, I. Shmuel, N. Wagner, E. Shoshan, and Y. C. Eldar, “Sub-nyquist radar prototype: Hardware and algorithm,” *IEEE Transactions on Aerospace and Electronic Systems*, vol. 50, no. 2, pp. 809–822, 2014.
- [10] Z. Wang, A. C. Bovik, H. R. Sheikh, and E. P. Simoncelli, “Image quality assessment: From error visibility to structural similarity,” *IEEE Transactions on Image Processing*, vol. 13, no. 4, pp. 600–612, 2004.